Universal level statistics in the presence of Andreev scattering

1995 J. Phys.: Condens. Matter 7 4033

(http://iopscience.iop.org/0953-8984/7/21/004)

J. Phys.: Condens. Matter 7 (1995) 4033–4050. Printed in the UK

Universal level statistics in the presence of Andreev scattering

J T Bruun†, S N Evangelou‡ and C J Lambert§

† Department of Mathematics and Statistics, Lancaster University, Lancaster, UK
‡ Department of Physics, University of Ioannina, Ioannina, 45 110, Greece
§ School of Physics and Materials, Lancaster University, Lancaster LA1 4YB, UK

Received 4 November 1994, in final form 13 March 1995

Abstract. We study the spectral eigenvalue statistics of tight-binding random matrix ensembles in the presence of Andreev scattering (AS). The nearest-level spacing distribution function is shown to follow a distribution $P_{AS}(s)$ which is distinct from the three well known Wigner–Dyson classes describing disordered 'normal' conductors. Numerical results for $P_{AS}(s)$ are obtained for a three-dimensional random tight-binding Hamiltonian and also for a two-dimensional transmission matrix, both including Andreev scattering. The $P_{AS}(s)$ distribution is also analytically reproduced and is shown to coincide with that obtained by folding a GOE metallic spectrum around $E = 0$.

1. Introduction

It is known [1–5], that statistical properties of electronic spectra in disordered metals can be understood by applying Wigner–Dyson random matrix theories (RMT). Such theories have a wide range of applicability extending to diverse areas of physics, the most recent of which is the quantum mechanical characterization of classically chaotic systems [6–10]. The reason for this general applicability can be traced to the fact that RMT focuses only on the symmetry of the original random matrix Hamiltonian, with real, symmetric matrices represented by the Gaussian orthogonal ensemble (GOE), complex Hermitian matrices by the Gaussian unitary ensemble (GUE) and self-dual quaternion random matrices by the Gaussian symplectic ensemble (GSE) [1–5]. The first of these arises in the absence of spin or magnetic fields [11–15] and explains statistical properties of the metallic spectra of electrons in random potentials, whereas if time reversal invariance is broken, for example by switching on a magnetic field, the resulting system is described by the GUE. Finally an electron with half-odd integer spin in a random potential with spin–orbit scattering represents a system associated with the GSE, which conserves the time reversal invariance but is not invariant under spin rotations. By convention, the three ensembles are classified by a universality class index β, which takes the values $\beta = 1$, 2 and 4 for the GOE, GUE and GSE respectively. Anderson localization corresponds to $\beta = 0$ and is not described by RMT, being associated with the tight-binding random matrix ensemble (TBRME) describing electrons in low-dimensional solids and/or large disorder [16]. Perhaps the most striking prediction of RMT is a universal reduction of mesoscopic conductance fluctuations by a factor $1/\beta$ when changing from GOE to one of the other universality classes [17].

A simple statistical quantity which can be used to distinguish between the three universality classes and also to characterize the localization properties of quantum

0953-8984/95/214033+18$19.50

Hamiltonian systems is the nearest-level spacing distribution function $P(s)$. For delocalized eigenfunctions in the presence of spin rotation or time reversal invariance, $P(s)$ obeys the well known Wigner surmise law $P_W(s) = (C_\beta s^\beta)\exp(-D_\beta s^2)$, where C_β and D_β are constants, chosen such that $P_W(s)$ is normalized and $\langle s\rangle = 1$. This form of $P_W(s)$ arises from the fact that the space filling delocalized eigenfunctions overlap each other, so that the corresponding eigenvalues exhibit level repulsion and the spectrum is smooth, rigid and correlated. When used to describe the eigenvalue statistics of transmission matrices belonging to disordered conductors [11–15], the above form of $P(s)$ immediately predicts the existence of universal conductance fluctuations in mesoscopic metallic systems. The correlated nature of the spectra corresponding to $\beta > 0$ is embodied in the small-s behaviour of $P_W(s)$, which takes the form $P_W(s) \propto s^\beta$ and therefore vanishes at $s = 0$. In contrast, pointlike localized eigenfunctions are non-overlapping in space and yield uncorrelated spectra with eigenvalues obeying normal Poisson statistics, $P(s) = \exp(-s)$. The association of delocalized states with Wigner–Dyson statistics and localization with Poisson statistics is quite rigorous and the point in the spectrum where the eigenvalues change their distribution [14, 15] coincides with the mobility edge.

All of the above results have been derived by studying normal systems only. For inhomogeneous conductors incorporating both normal and superconducting regions recent experiments and theoretical work [19, 18] have shown that coherent transport phenomena, such as universal conductance fluctuations, can also be observed. In this paper we consider the less understood case of spectral fluctuations in the presence of superconductivity, where normal state transport theory must be generalized [20, 21] to account for the absence of quasiparticle charge conservation. This is due to the phenomenon of Andreev scattering (AS) [22] whereby a quasiparticle, incident on a superconducting surface from a normal material, can be reflected into its time-reversed counterpart. Recently superconductivity-induced Anderson localization was found in one-dimensional systems [23] but not in two dimensions, where a line of critical points was obtained [24]. In what follows we show that in the presence of Andreev scattering, both the mesoscopic and the localization descriptions become inappropriate and a distribution $P_{AS}(s)$ emerges which is distinct from both the Wigner and Poisson distributions appropriate to normal conductors. It is shown that this novel distribution survives in the presence of weak diagonal disorder and turns into a Poisson distribution for strong disorder, indicating the presence of a localization transition.

2. The random matrix models

In this section, we briefly summarize some common classes of random matrices, whose spectra are described by RMT and write down generalizations of these in the presence of AS. The simplest example is a random matrix belonging to the GOE, which, in terms of an arbitrary orthogonalized basis set ($|n\rangle, n = 1, 2, .., N$), is of the form

$$\mathbf{H}_0 = \sum_{n=1}^{N}\sum_{m=1}^{N} H_{n,m}|n\rangle\langle m|. \tag{1}$$

The matrix elements $H_{n,m} = H^*_{m,n} = H_{m,n}$ are independent identically distributed random variables, chosen from a Gaussian probability distribution of mean zero and fixed variance. The GOE is exactly solvable for both ensemble-averaged properties, such as the averaged density of states $\langle\rho(E)\rangle$ which is approximated by a simple semicircle law and for the nearest-level spacing distribution function $P(s)$ approximated by the Wigner surmise [1–5]. It is interesting that the form of the $P(s)$ function can be obtained by diagonalizing matrices of size as small as 2×2 [3].

The above matrix differs from tight-binding Hamiltonian matrices used to describe electrons in disordered solids, since the latter typically possess only nearest-neighbour, off-diagonal couplings. For this reason, the GOE does not describe phenomena such as Anderson localization [16]. For electrons in disordered solids, the appropriate matrix representation is the TBRME [11–15], which in the absence of spin effects consists of random real and symmetric matrices, which are both short ranged and sparse, reflecting the finite range of the interactions. Such matrices are of the form

$$\mathbf{H}_0 = \sum_n e_n |n\rangle\langle n| + \sum_{(n,m)} V_{n,m} |n\rangle\langle m| \tag{2}$$

where n labels all the $N = L^d$ sites of a d-dimensional lattice with linear size L and the second sum is taken over all nearest-neighbour pairs (n, m) on the lattice. Usually one deals with a closed sample, with boundaries impermeable to electrons, so that the spectrum is discrete. The random on-site potential e_n is a uniformly distributed random variable, from $-W/2$ to $W/2$, while $V_{n,m}$ are off-diagonal matrix elements of magnitude unity ($V_{n,m} = 1$). For $E = 0$ eigenfunctions the critical disorder is $W_c \simeq 16.5$ in $d = 3$, with all states becoming localized for $W > W_c$. The GOE limit is strictly approached by the TBRME only for infinite space dimensionality $d = \infty$, when both the diagonal (ϵ_n) and off-diagonal ($V_{n,m}$) matrix elements are randomly chosen from appropriate probability distributions. However in the presence of weak disorder, even for finite d, the GOE can effectively replace the TBRME, since the TBRME for small W and $d > 2$ has random delocalized states, which are described by the Wigner–Dyson statistics. Therefore, in the mesoscopic regime all the known results for the GOE carry through and explain the measurable fluctuation phenomena in metallic conductors of size smaller than other characteristic decay lengths [11–15]. In the presence of Andreev scattering (AS) generated by spin singlet, local s-wave pairing, the Hamiltonian which appears in the Bogoliubov–de Gennes (BDG) equation has the form

$$\mathbf{H} = \begin{pmatrix} \mathbf{H}_0 & \boldsymbol{\Delta} \\ \boldsymbol{\Delta}^* & -\mathbf{H}_0^* \end{pmatrix} \tag{3}$$

where $\boldsymbol{\Delta}$ is a diagonal order parameter matrix with elements Δ_n. In what follows we examine three distinct examples: (i) a normal system with $\Delta_n = 0$ for all n, (ii) homogeneous superconductivity for which $\Delta_n = \Delta_0 =$ constant and (iii) the inhomogeneous superconducting case for which $\Delta_n = \Delta_0 \exp(i\theta_n)$, where θ_n is a random variable uniformly distributed between $-\pi$ and π.

3. The level spacing distribution function $P_{AS}(s)$ in the presence of Andreev scattering

In order to understand the nature of the fluctuations in the presence of AS we first derive the level spacing distribution $P^0_{AS}(s)$ for the smallest possible matrix describing a homogeneous superconductor with more than one particle degree of freedom. The smallest such random matrix is of the form of equation (3), with

$$\mathbf{H}_0 = \begin{pmatrix} H_{11} & H_{12} \\ H_{12} & H_{22} \end{pmatrix} \tag{4}$$

and

$$\boldsymbol{\Delta} = \begin{pmatrix} \Delta_0 & 0 \\ 0 & \Delta_0 \end{pmatrix} \tag{5}$$

where H_{11}, H_{12} and H_{22} are Gaussian random variables with zero mean and variance $\sigma^2 = 1$. The eigenvalues of $\mathbf{H}_0$ are

$$\epsilon_{\pm} = \frac{(H_{11} + H_{22})}{2} \pm \frac{\sqrt{(H_{11} - H_{22})^2 + 4H_{12}^2}}{2} \tag{6}$$

and the corresponding eigenvalues of $\mathbf{H}$

$$E_i = \pm\sqrt{\epsilon_{\pm}^2 + |\Delta_0|^2}. \tag{7}$$

If the indices i label the four eigenvalues in ascending order, then the level spacings are

$$S_i = E_{i+1} - E_i. \tag{8}$$

In what follows, we derive the distribution $P_{\mathrm{AS}}^0(s)$ for the corresponding normalized spacings s_i, defined by

$$s_i = S_i/\langle S\rangle. \tag{9}$$

The first step in the derivation is to show that for a large system, the relative level spacing s_i in the superconductor is identical to that obtained by setting $\Delta_0 = 0$, where the resulting spectrum ϵ_i is obtained by adding the eigenvalues of $\mathbf{H}_0$ to those of $-\mathbf{H}_0$. This folded spectrum has spacings $S_i^0 = (\epsilon_{i+1} - \epsilon_i)$ and will be shown to possess a distribution, distinct from both Poisson and Wigner statistics.

To this end one notes that from equation (7),

$$E_{i+1}^2 - E_i^2 = \epsilon_{i+1}^2 - \epsilon_i^2 \tag{10}$$

and hence

$$(E_{i+1} - E_i) = (\epsilon_{i+1} - \epsilon_i)\left(\frac{\epsilon_{i+1} + \epsilon_i}{E_{i+1} + E_i}\right).$$

In the limit of a large number of levels, where the spacings between adjacent levels tend to zero, $\epsilon_{i+1} \simeq \epsilon_i$ and $E_{i+1} \simeq E_i$. Hence

$$(E_{i+1} - E_i) \simeq (\epsilon_{i+1} - \epsilon_i)\frac{\epsilon_i}{E_i}. \tag{11}$$

The density of states in the normal system $n_0(\epsilon)$ is related to the density of states $n(E)$ of the homogeneous superconductor through the equality

$$n_0(\epsilon)\,\mathrm{d}\epsilon = n(E)\,\mathrm{d}E. \tag{12}$$

Hence from equation (7),

$$\frac{n_0(\epsilon)}{n(E)} = \frac{\epsilon_i}{E_i}. \tag{13}$$

Substituting this into equation (11) yields

$$(E_{i+1} - E_i) \simeq (\epsilon_{i+1} - \epsilon_i)\frac{n_0(\epsilon_i)}{n(E_i)} \tag{14}$$

or, in terms of the level spacings,

$$S_i n(E_i) \simeq S_i n_0(\epsilon_i). \tag{15}$$

Since the mean level spacings are simply the reciprocal of the density of states, $\langle S_i\rangle = 1/n(E_i)$ and $\langle S_i^0\rangle = 1/n_0(\epsilon_i)$, one obtains for the relative spacings

$$\frac{S}{\langle S\rangle} = \frac{S^0}{\langle S^0\rangle} \tag{16}$$

or equivalently

$$s_i = s_i^0. \tag{17}$$

This proves that the relative level spacings of a normal folded spectrum are identical to those of the BDG Hamiltonian with a uniform order parameter. As a consequence one need only study the folded spectrum of $\mathbf{H}_0$ in order to determine the level density function $P_{AS}(s)$ for the superconducting system. From equation (6), the two energy levels of $\mathbf{H}_0$ are

$$\epsilon_\pm = \frac{\alpha}{2} \pm \frac{\delta}{2} \tag{18}$$

where

$$\alpha = H_{11} + H_{22} \tag{19}$$

and

$$\delta = \sqrt{(H_{11} - H_{22})^2 + 4H_{12}^2}. \tag{20}$$

The level spacing is simply $S = \delta$, and has been discussed in detail elsewhere [17]. In contrast, the folded spectrum corresponds to the the two levels $\epsilon_\pm$ and their partners $-\epsilon_\pm$. As shown in figure 1, four distinct combinations can now arise, depending on the relative values of α and δ. In each case, there are two distinct level spacings, S_1 and S_2, with the spacing S_1 occurring twice as often as S_2. The corresponding values of S_i are shown in the table 1.

Table 1. The folded spacings.

Figure 1	$S_1(\alpha, \delta)$	$S_2(\alpha, \delta)$	Range of α
(i)	δ	$\alpha - \delta$	$\alpha > \delta$
(ii)	δ	$-(\alpha + \delta)$	$\alpha < -\delta$
(iii)	α	$-(\alpha - \delta)$	$0 < \alpha < \delta$
(iv)	$-\alpha$	$\alpha + \delta$	$-\delta < \alpha < 0$

To obtain the distribution P_{AS} of this folded spectrum we write $\gamma = H_{11} - H_{22}$ and make a transformation from (H_{11}, H_{22}, H_{12}) to (α, δ, γ). Since H_{11}, H_{22} and $H_{12} = H_{21}$ are Gaussian variables with joint distribution $P(H_{11}, H_{22}, H_{12}) = (2\pi\sigma^2)^{-3/2} \exp\{-[H_{11}^2 + H_{22}^2 + H_{12}^2]/(2\sigma^2)\}$ and the Jacobian of the transformation is $|\delta/8H_{12}|$, this yields for the joint distribution of (α, δ, γ)

$$P(\alpha, \delta, \gamma) = \frac{\delta\Theta(\delta^2 - \gamma^2)}{2(2\pi\sigma^2)^{3/2}(\delta^2 - \gamma^2)^{1/2}} \exp\{-[\alpha^2 + \gamma^2 + \delta^2/2]/4\sigma^2\} \tag{21}$$

where $\Theta(x)$ is the Heaviside function. Integrating over all γ yields

$$P(\alpha, \delta) = P(\alpha)P(\delta) \tag{22}$$

where

$$P(\alpha) = (4\pi\sigma^2)^{-1/2} \exp\{-\alpha^2/4\sigma^2\} \tag{23}$$

and

$$P(\delta) = \frac{f(\delta)}{2\pi\sigma^2\sqrt{2}} \exp\{-\delta^2/8\sigma^2\} \tag{24}$$

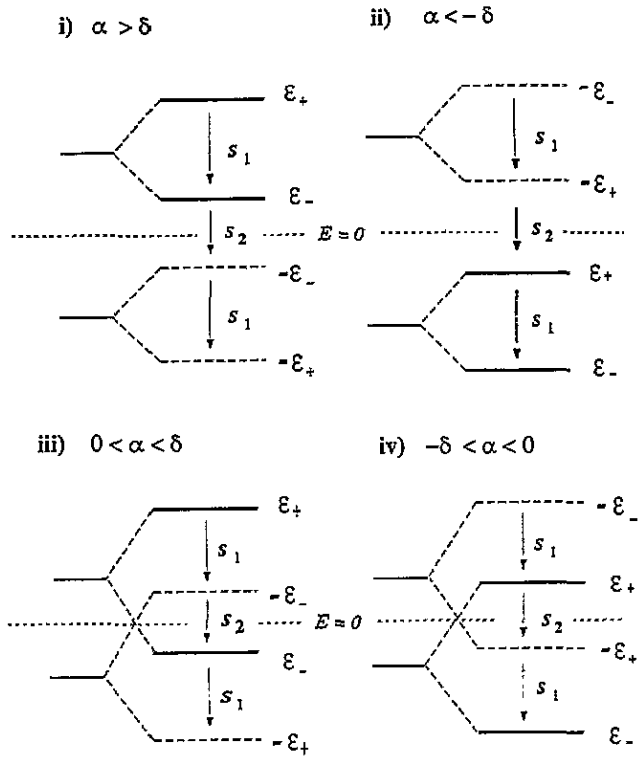

Figure 1. A folded two-level system.

where, after writing $\gamma = \delta \sin\theta$,

$$f(\delta) = \delta \int_{-\pi/2}^{\pi/2} \mathrm{d}\theta \exp\{-\delta^2 \sin^2\theta/8\sigma^2\} = \pi\delta \exp\{-\delta^2/16\sigma^2\} J_0(-\mathrm{i}\delta^2/16\sigma^2) \tag{25}$$

with $J_0(z)$ a zeroth-order Bessel function of the first kind. This yields $f(\delta) \approx \pi\delta$ for small δ and $f(\delta) \approx (8\pi\sigma^2)^{1/2}$ for large δ.

In table 1, situations (i) and (iii) corresponding to $\alpha \geqslant 0$ are identical to possibilities (ii) and (iv) with $\alpha \leqslant 0$ and therefore only positive α need be considered explicitly. Since the distributions of the level spacings S_1 and S_2 are given by

$$P_i(S) = \int\int \mathrm{d}\alpha\, \mathrm{d}\delta\ \delta(S_i(\alpha,\delta) - S) P(\alpha) P(\delta) \tag{26}$$

one finds

$$P_1(S_1) = 2\int_0^\infty \int_0^\infty \mathrm{d}\alpha\, \mathrm{d}\delta P(\alpha) P(\delta) \{\Theta(\alpha-\delta)\,\delta(\delta - S_1) + \Theta(\delta-\alpha)\,\delta(\alpha - S_1)\} \tag{27}$$

and

$$P_2(S_2) = 2\int_0^\infty \int_0^\infty \mathrm{d}\alpha\, \mathrm{d}\delta P(\alpha) P(\delta) \{\Theta(\alpha-\delta)\,\delta(\alpha - \delta - S_2) + \Theta(\delta-\alpha)\,\delta(\delta - \alpha - S_2)\}. \tag{28}$$

Given that S_1 occurs twice as often as S_2, the distribution of S is

$$P^0_{AS}(S) = \tfrac{2}{3}P_1(S) + \tfrac{1}{3}P_2(S). \tag{29}$$

After evaluating the integrals numerically, the distributions for the normalized spacing $s = S/\langle S\rangle$, namely $P^0_{AS}(s) = \langle S\rangle P_{AS}(S)$, $P_1(s) = \langle S\rangle P_1(S)$ and $P_2(s) = \langle S\rangle P_2(S)$, are as shown in figure 2(a). As an aside, it is interesting to note that for the purpose of computing $P^0_{AS}(s)$, the distribution $P(\delta)$ of equation (24) is approximately given by $p(\delta) = [\delta/(3\sigma^2)]\exp\{-[\delta^2/(6\sigma^2)]\}$. Figure 2(b) shows a comparison between this approximate form and the exact result (24). In the integrals on the right-hand side of equations (27) and (28), if this approximate from were used instead of (24), then on the scale of the line thickness used in figure 2(a), the result for $P^0_{AS}(s)$ is found to be unchanged.

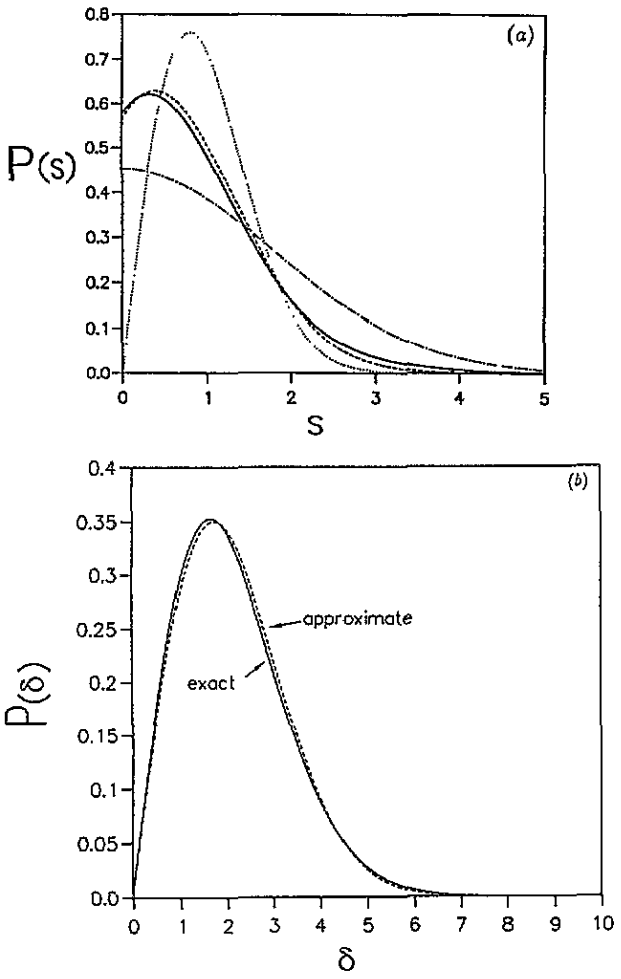

Figure 2. Figure 2(a) shows the predicted distributions for the folded spectra: $P^0_{AS}(s)$ (solid line), $P_1(s)$ and $P_2(s)$ (dashed and dash–dotted respectively). The GOE statistic (dotted line) is shown for comparison. The solid line of figure 2(b) shows a plot of the right-hand side of equation (24), while the dashed line is a plot of the function $[\delta/(3\sigma^2)]\exp\{[-\delta^2/(6\sigma^2)]\}$.

In what follows we refer to $P^0_{AS}(s)$ as the folded distribution of the two-level system described by $\mathbf{H}_0$ and compare this with the distribution $P_{AS}(s)$ obtained by folding a GOE

spectrum. To this end we now present results obtained by numerically diagonalizing $N \times N$ symmetric matrices of the form shown in equation (1). The method of calculation relies on the numerical computation of the eigenvalues E_j, with $j = 1, 2, ..., N$ obtained from the finite-size matrices $\mathbf{H}$ in the appropriate matrix ensemble. Then by allowing the matrix size N to vary we determine the large-N behaviour. $P(s)$ can be numerically obtained by considering the distribution of the differences $\langle \mathcal{N}(E_{j+1}) \rangle - \langle \mathcal{N}(E_j) \rangle = (E_{j+1} - E_j)(\partial/\partial E)\langle \mathcal{N}(E) \rangle$, where $\langle \mathcal{N}(E) \rangle$ is the averaged integrated DOS at the energy E. Our numerical results for normal systems agree well with the Wigner surmise and the Poisson law for the delocalized and the localized phases, respectively [11–15]. An intermediate-scale invariant distribution which interpolates between the two limits was obtained in this critical case [14]. Figure 3 shows the distribution $P(s)$ of the unfolded spectrum of $\mathbf{H}_0$, obtained from 1000 realizations of matrices of size $N = 50$. The GOE (dashed line) and Poisson (dotted) distributions are shown for comparison. Figure 4 shows results for the folded spectrum of $\mathbf{H}_0$. The numerical result for the distribution $P_{AS}(s)$ is the somewhat noisy solid line of figure 4. This distribution was obtained by diagonalizing matrices of size $N = 100$ and an ensemble of 10 000 realizations. On the same graph, the analytical result $P^0_{AS}(s)$ of equation (29) is shown as a solid black line and for comparison the dotted line shows the Wigner distribution $P_W(s)$. It is immediately apparent that the two-level folded distribution $P^0_{AS}(s)$ yields the qualitative features of the large-N spectrum $P_{AS}(s)$.

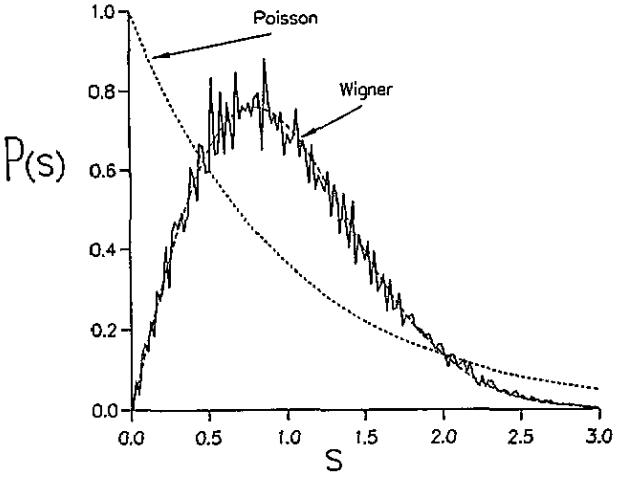

Figure 3. The computed distribution for a symmetric Hamiltonian (unfolded) of the form shown in equation (1). The matrix dimension is $N = 50$ and 1000 realizations of the system were used. For comparison the dashed and dotted lines show GOE and Poisson distribution.

The distributions obtained by folding GOE, GUE, GSE and TBRME spectra are the replacements of the unfolded spectra in the presence of Andreev scattering. In figure 5 we illustrate results for the TBRME in $d = 3$ obtained for lattices of size L^d with $L = [6, 8, 10]$, disorders $W = 10$ and 30. The statistics were obtained from an ensemble of 10 000 or more random matrices. The order parameter was fixed in each case to $\Delta_0 = 0.1$ and the energies varied over a narrow window about $E = 0$. From the size variation we obtain the universal curve P_{AS} for $W = 10$ (figure 5(a)) and asymptotically the Poisson $\exp(-S)$ law in the case of $W = 30$ as shown in figure 5(b). This indicates that in the presence of Andreev scattering, the Anderson transition occurs at a value of W greater than the normal critical disorder $W_c = 16.5$.

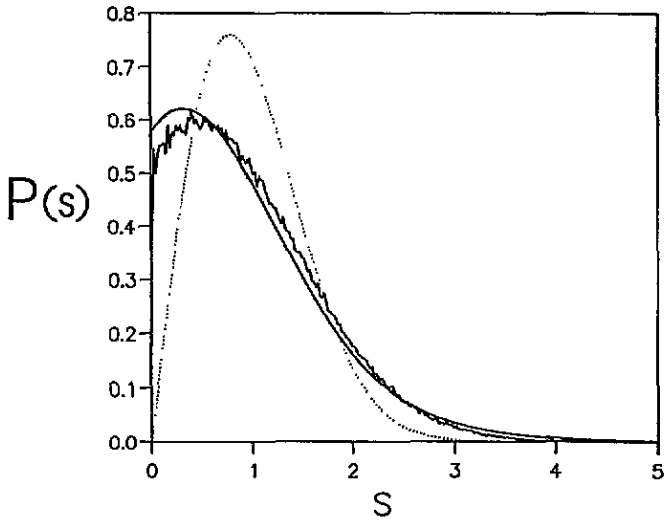

Figure 4. The noisy solid line shows the distribution $P_{AS}(s)$ for the folded spectrum of a Gaussian random symmetric Hamiltonian, obtained from 10000 realizations of matrices of size $N = 100$. The smooth solid line shown is the analytical curve for the two-level folded system $P_{AS}^{0}(s)$. For comparison the dotted line shows the GOE distribution.

4. The transmission eigenvalue spectrum

Having demonstrated that the level spacings of the BDG operator possess a new distribution, which is distinct from the well known Wigner and Poisson distributions, we now examine the level statistics of the generalized transmission matrix product $\mathbf{t}'\mathbf{t}'^{\dagger}$, where $\mathbf{t}'$ is the general transmission matrix for a multichannel two-probe conductor that incorporates both normal and Andreev scattering. This matrix is obtained from the full scattering matrix $\mathbf{S}(E)$ which has the structure

$$\mathbf{S}(E) = \begin{bmatrix} \mathbf{r} & \mathbf{t}' \\ \mathbf{t} & \mathbf{r}' \end{bmatrix}. \tag{30}$$

The submatrix $\mathbf{t}'$ which characterizes transmission from one side of the scatterer to the other has the form

$$\mathbf{t}'(E) = \begin{bmatrix} t_{pp'} & t_{ph'} \\ t_{hp'} & t_{hh'} \end{bmatrix} \tag{31}$$

where if $m^{\beta}(E)$ is the number of propagating channels for excitations of type β ($\beta = +1$ for particles, -1 for holes), the subblocks have dimensions $m^{+}(E) \times m^{+}(E)$ for $t_{pp'}$, $m^{+}(E) \times m^{-}(E)$ for $t_{ph'}$, $m^{-}(E) \times m^{+}(E)$ for $t_{hp'}$ and $m^{-}(E) \times m^{-}(E)$ for $t_{hh'}$. The eigenvalues of this matrix are $\{e_i: i = 1, 2, ..., m^{+}(E) + m^{-}(E)\}$ and lie in the range $0 \leqslant e_i \leqslant 1$. For convenience these transmission eigenvalues are arranged so that $e_1 < e_2 < ... < e_{[m^{+}(E)+m^{-}(E)]}$. For a normal system they are related to the the two-probe conductance G via

$$G = \mathrm{Tr}\,\mathbf{t}'\mathbf{t}'^{\dagger} = \sum_{i=1}^{m^{+}(E)+m^{-}(E)} e_i. \tag{32}$$

In what follows the scattering matrix of square tight-binding systems will be evaluated numerically using the technique outlined in appendix 1 of [21]. The systems are described

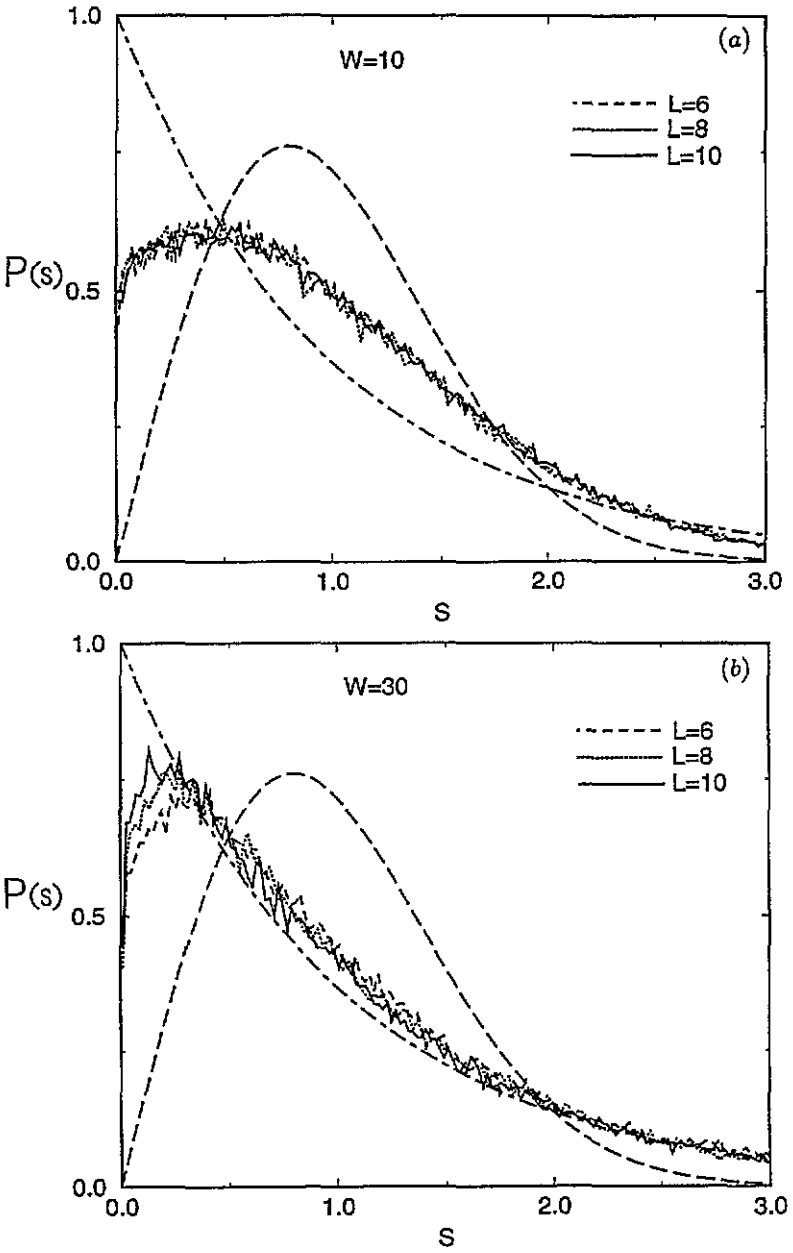

Figure 5. The results for the TBRME in $d = 3$ dimensions in the presence of Andreev scattering for disorder strengths corresponding to delocalized ($W = 10$) (a) and localized ($W = 30$) values (b). Results for three system sizes L^d with $L = [6, 8, 10]$ are shown. The horizontal axis has units of the local mean level spacing and the smooth curves are the GOE (dashed line) and Poisson distributions (dot–dashed line).

by equation (3), with $\mathbf{H}_0$ given by equation (2) and results for the three examples introduced at the end of section 2 will be presented. In each case, diagonal disorder W is present, but there is no disorder in the magnitude of Δ. In the first set of results, the behaviour of a 10×10 square is considered. The disorder is fixed to the value $W = 1$, so that the

system is diffusive in nature. For the normal model, the energy E is varied and in the two superconducting models both E and Δ_0 are varied. For the range of E studied, there are nine particle and hole propagation channels, i.e. $m^+(E) = m^-(E) = 9$.

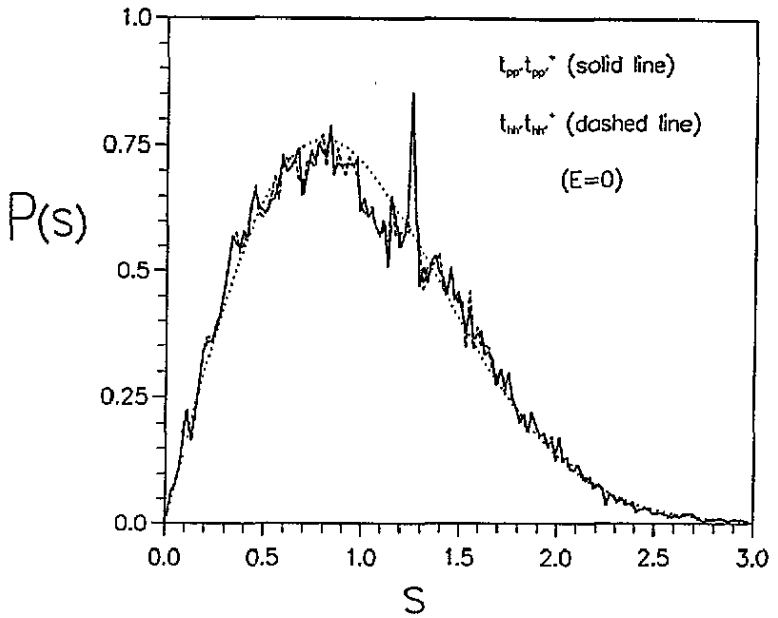

Figure 6. Degenerate distributions of transmission eigenvalue spacings for the particle–particle (solid line) and hole–hole (dashed) matrices of a normal system. These results were obtained for 10×10 squares, with disorder $W = 1$, $E = 0$ and 5000 realizations. The dotted line shows the GOE distribution.

Figure 6 shows results for a normal system ($\Delta_0 = 0$), obtained from 5000 realizations at $E = 0$. In this case, the particle and hole degrees of freedom are decoupled and therefore the transmission eigenvalues of the particle–particle or hole–hole matrices $t_{pp'}t_{pp'}^\dagger$ and $t_{hh'}t_{hh'}^\dagger$ should separately exhibit GOE statistics. Figure 6 shows results for the spectral properties of the separate matrices $t_{pp'}t_{pp'}^\dagger$ and $t_{hh'}t_{hh'}^\dagger$ respectively and that the two distributions, to within numerical accuracy, are degenerate and coincide with a GOE. This degeneracy is guaranteed by particle–hole symmetry at $E = 0$. As a consequence, after combining the transmission eigenvalues for the two degenerate systems, the level statistics for $\mathbf{t}'\mathbf{t}'^\dagger$ take the form of a standard GOE plus a Dirac δ function at $s = 0$. In what follows this combined distribution will be denoted DGOE. At $E \neq 0$, particles and holes are no longer degenerate and the combined spectrum of $\mathbf{t}'\mathbf{t}'^\dagger(E)$ is no longer of the form DGOE. Figure 7 shows the combined spectrum of the normal system used in figure 6, except that $E = 0.15$ and 1000 realizations were used. Since $\Delta_0 = 0$, the distribution shown in figure 7 is obtained by combining the spectrum of $t_{pp'}t_{pp'}^\dagger$ with that of $t_{hh'}t_{hh'}^\dagger$. For comparison the smooth line through the graph is the analytic two-level approximation $P_{AS}^0(s)$. These results indicate that the folded distribution $P_{AS}^0(s)$ describes the qualitative features of the transmission eigenvalue spectrum, provided the degeneracy due to particle–hole symmetry is lifted. As a consequence of this change in statistic, there will be a crossover from a $P_{AS}(s)$ distribution to a DGOE as the energy E tends to zero. An example of this crossover is given in figure 8, which shows results for two energies $E = 0.15$ and 0.005.

Unlike the spectrum of H, there is no reason to suppose that the level spacing distribution

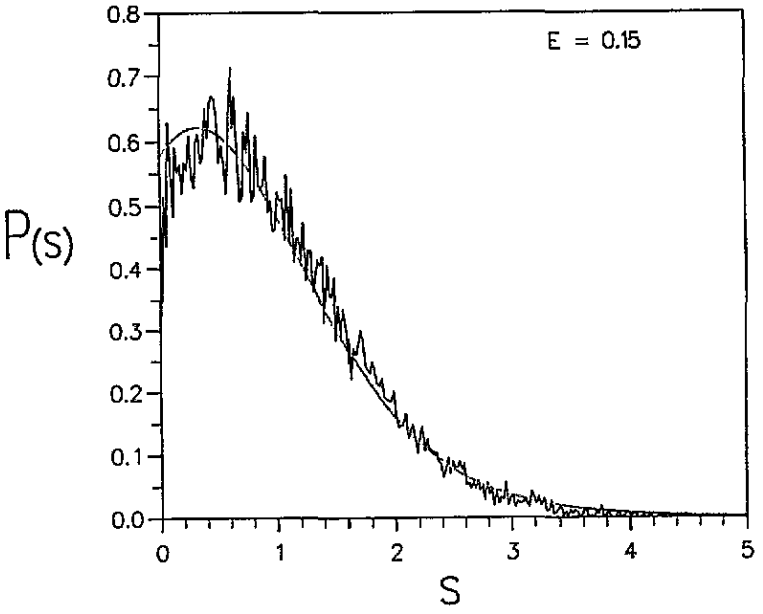

Figure 7. Transmission eigenvalues of $t't'^{\dagger}$, with $\Delta_0 = 0$. Parameter values are as for figure 6, except $E = 0.15$ and 1000 realizations. For comparison the smooth line shows $P^0_{AS}(s)$.

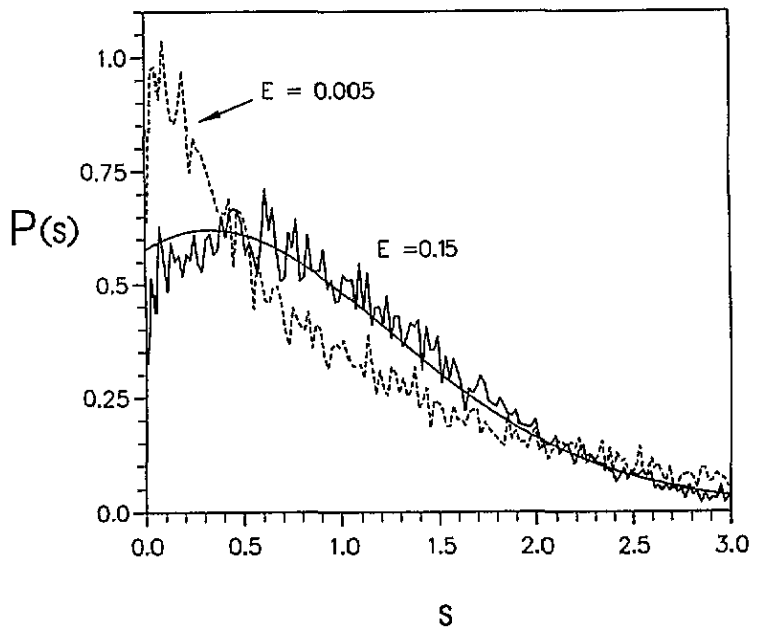

Figure 8. This figure shows the crossover from SFD to DGOE. Parameter values are as for figure 7. Results for two energies are shown, $E = 0.15$ and $E = 0.005$.

of the transmission eigenvalues is independent of Δ_0. Therefore having considered the case $\Delta_0 = 0$ we now present a selection of results for systems with diagonal disorder $W = 1$, but with a uniform order parameter. Figure 9 shows results obtained from 1000 realizations

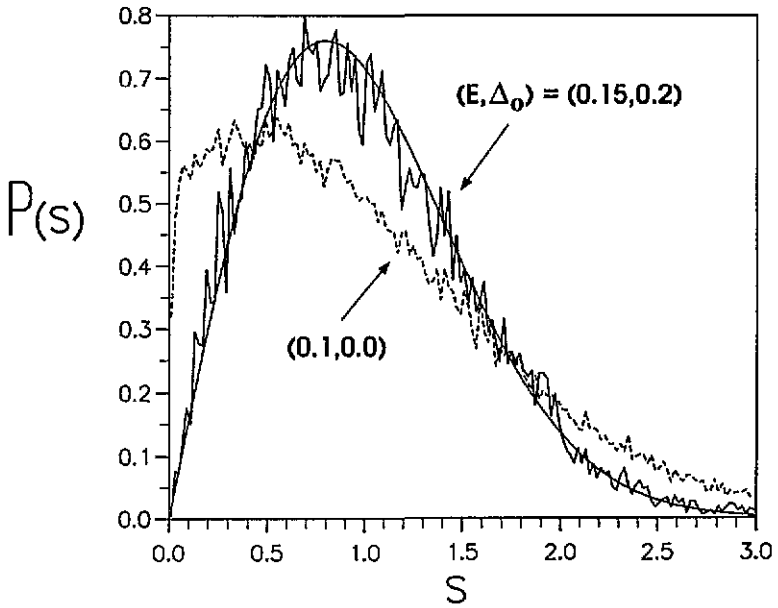

Figure 9. The distribution of transmission eigenvalue spacings $P(s)$ for a homogeneous superconductor. For these calculations, $M = 10$, $W = 1$ and 1000 realizations were used. Two different systems are depicted, $(E, \Delta_0) = (0.15, 0.2)$ as the solid fluctuating line and $(0.1, 0.0)$ as the dashed line.

of a system with $(E, \Delta_0) = (0.15, 0.2)$. For comparison the smooth line is this figure is the GOE distribution. The statistic of s for this choice of (E, Δ_0) can thus be identified with the GOE, which implies that as Δ_0 increases from zero there is a crossover from the $P_{AS}(s)$ statistics of the normal-disordered $E \neq 0$ conductor shown in figure 8 to the GOE shown in figure 9. Also shown in this figure as the dashed line is a distribution obtained with $(E, \Delta_0) = (0.1, 0)$. The above transition from GOE to $P_{AS}(s)$ occurs for $E > 0$, with increasing Δ_0. Since particle–hole symmetry at $E = 0$ forces the spectrum to be doubly degenerate, there must also be a transition from GOE to DGOE for $\Delta_0 > 0$, but $E \to 0$. Examples of this transition are presented in figure 10, which shows distributions for $(E, \Delta_0) = (0.15, 0.1)$ (solid line) and $(E, \Delta_0) = (0.01, 0.1)$ (dashed line).

Having considered the case of a homogeneous order parameter, we now examine the case of an inhomogeneous superconductor for which $\Delta_n = \Delta_0 \exp(i\theta_n)$, where θ_n is a random variable uniformly distributed between $-\pi$ and π. Figure 11 shows results obtained from 1000 realizations of a system with $(E, \Delta_0) = (0.22, 0.22)$. For comparison, since this model breaks time reversal symmetry, the smooth line shows the GUE distribution. As $\Delta_0 \to 0$, time reversal symmetry is restored and therefore one expects a GUE to $P_{AS}(s)$ crossover to occur. This is illustrated in figure 12, for three sets of parameters which have a common energy and varying Δ_0 as $(E, \Delta_0) = (0.1, 0.2)$, $(0.1, 0.06)$ and $(0.1, 0.0)$ corresponding to the solid, dotted and dashed lines respectively. Similarly as $E \to 0$, particle–hole symmetry forces a double degeneracy on the spectrum. As a consequence a GUE to GUE + δ function (DGUE) transition takes place, as illustrated in figure 13, which shows results for $(E, \Delta_0) = (0.1, 0.2)$ as the solid line and $(0.01, 0.2)$ as the dashed line.

The above results demonstrate that as the pair of parameters (E, Δ_0) is varied the level statistics varies between a small number of limiting distributions. To summarize this

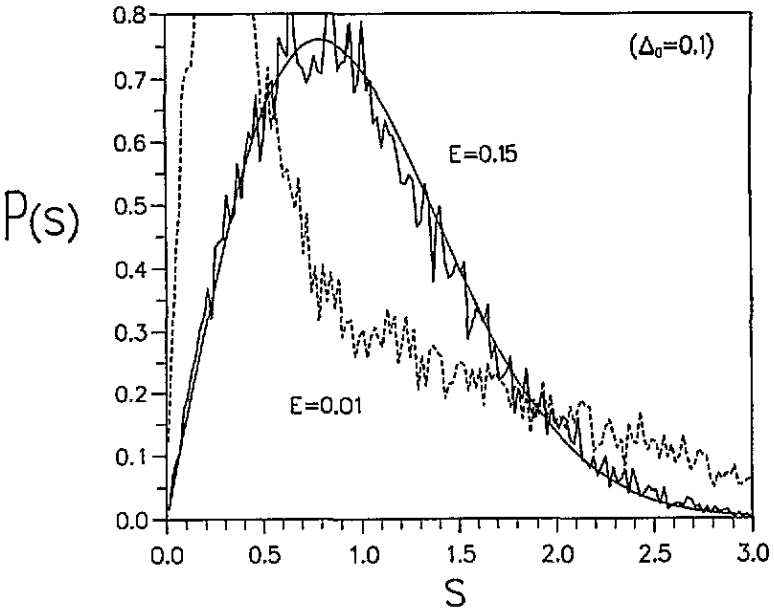

Figure 10. As for figure 9, but with $(E, \Delta_0) = (0.15, 0.1)$, the solid line, and $(0.01, 0.1)$, the dashed line.

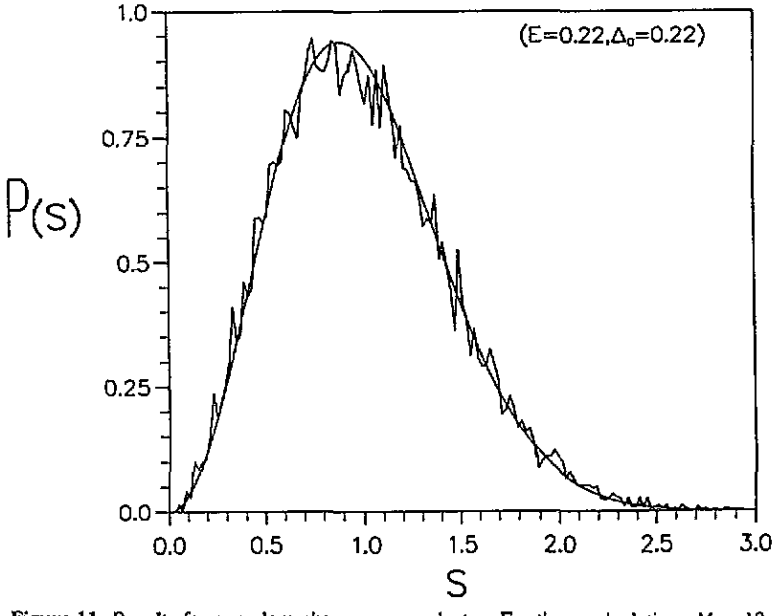

Figure 11. Results for a random phase superconductor. For these calculations $M = 10$, $W = 1$, $(E, \Delta_0) = (0.22, 0.22)$ and 1000 realizations were used.

behaviour, it is useful to identify boundaries in the (E, Δ_0) plane, which determine the crossover from one distribution to another. To define these boundaries, we have used the standard deviations of the numerically obtained distributions as the natural measure with which one can quantify the regions of distinct statistical behaviour. The standard deviations

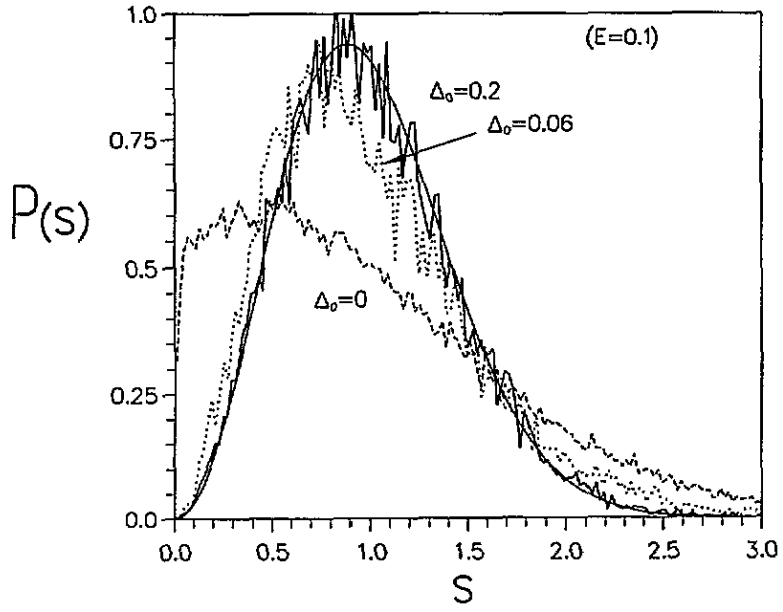

Figure 12. Results for a random phase superconductor showing the GUE → SFD transition. For these calculations, 1000 realizations were used, $M = L = 10$, $W = 1$ with $(E, \Delta_0) = (0.1, 0.2)$, $(0.1, 0.06)$ and $(0.1, 0.0)$ depicted with the solid, dotted and dashed lines respectively.

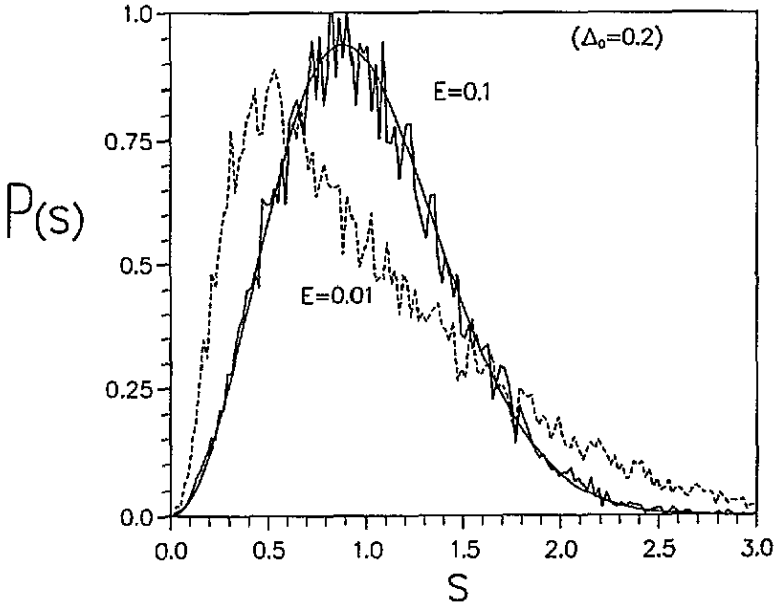

Figure 13. Results for a random phase superconductor showing the GUE → DGUE transition. For these calculations, 1000 realizations were used, $M = L = 10$, $W = 1$. Two densities for $(E, \Delta_0) = (0.1, 0.2)$, the solid line, and $(0.01, 0.2)$, the dashed, are shown.

σ_{AS}, σ_{GOE} and σ_{GUE} are shown in table 2, along with the value σ^0_{AS} for the two-level folded distribution $P^0_{AS}(s)$.

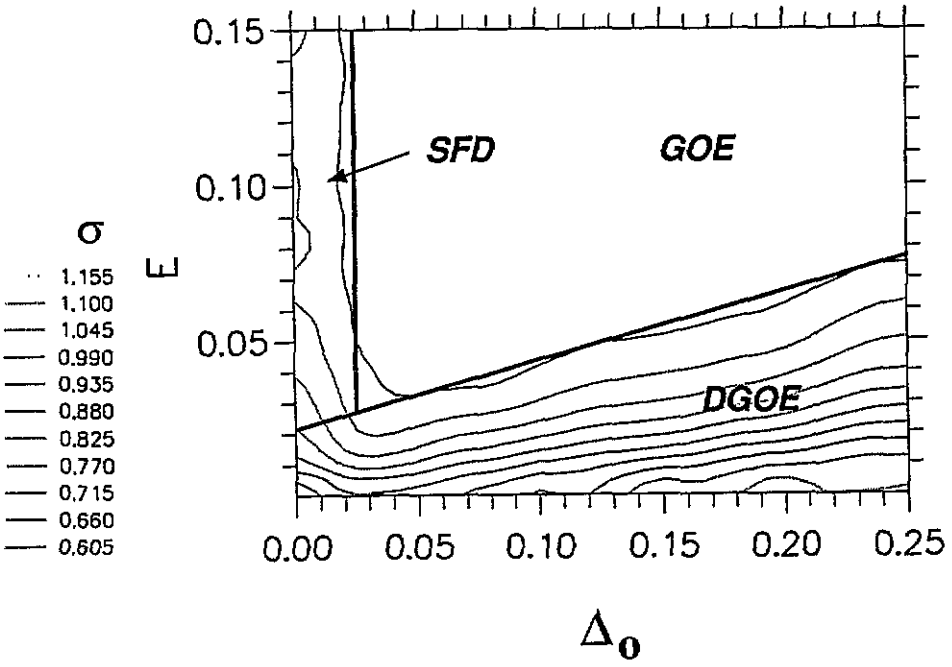

Figure 14. Contours of constant standard deviation for the distribution of transmission eigenvalue spacings of a homogeneous superconductor. The solid lines are the estimates of the boundaries between regions occupied by different limiting distributions. The value of σ for the contour which intersects the $\Delta_0 = 0.25$ axis at the highest value of E is 0.605. The contour intersecting this axis at the next-highest value of E corresponds to $\sigma = 0.660$. Table 2 shows the values of σ associated with these and the other contours.

In what follows, all results for σ are calculated from an ensemble of 1000 realizations of 10×10 squares, with $W = 1$. Figure 14 shows results for the contours of constant σ for a homogeneous superconductor with a real order parameter. The thick solid lines are crude estimates of the boundaries at which a crossover from one distribution to another occurs. The regions occupied by the three distributions, namely GOE, SFD and DGOE are marked in the figure. Figure 15 shows the corresponding results obtained in the presence of random order parameter phases, uniformly distributed over $\pm\pi$. In this case the thick solid lines are estimates of the boundaries between regions occupied by four different distributions, namely GUE, SFD, DGUE and DGOE.

5. Discussion

In this paper, we have reported the results of a study of the spectral eigenvalue statistics of the Bogoliubov–de Gennes Hamiltonian and of the associated transmission matrix $\mathbf{t}'\mathbf{t}'^{\dagger}$. The nearest-level spacing distribution function $P(s)$ has been evaluated numerically for both a folded symmetric random Hamiltonian $\mathbf{H}_0$ and the transmission matrix $\mathbf{t}'\mathbf{t}'^{\dagger}$. We have shown that in the presence of Andreev scattering, a distribution $P_{AS}(s)$ emerges which describes the level density fluctuations of mesoscopic superconductors. An approximation to this distribution has been obtained by folding the metallic spectrum of a two-level system about $E = 0$. We have also examined the folded spectrum of a TBRME in three dimensions. As the disorder is increased, this crosses over from a GOE folded spectrum described

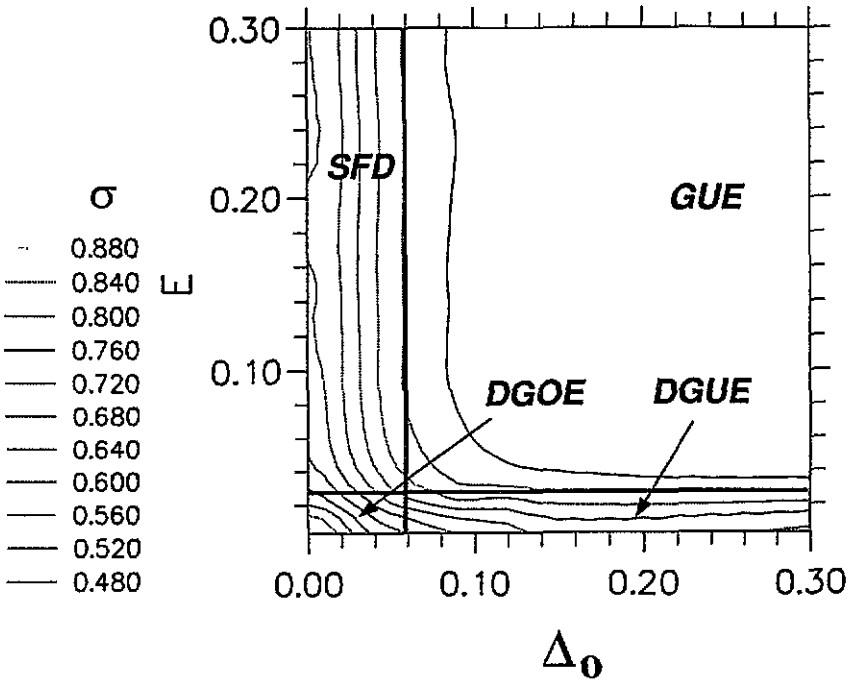

Figure 15. As for figure 14, but for an order parameter with random phases.

by $P_{AS}(s)$ to a Poisson distribution, but only at much larger values of disorder than the corresponding normal system. This indicates that the presence of a homogeneous order parameter suppresses Anderson localization.

Table 2. Standard deviations σ of various distributions.

Constant	GOE	GUE	P_{AS}	P_{AS}^{0}
σ	$\sigma_{GOE} =$ 0.523	$\sigma_{GUE} =$ 0.422	$\sigma_{AS} =$ 0.706	$\sigma_{AS}^{0} =$ 0.779

For simplicity we have restricted the analysis to the level spacing distribution $P(s)$. For the future it will be of interest to verify the universality of the new folded distribution for other eigenvalue statistical measures such as the number variance and the two-point correlation function. It is also of interest to obtain a detailed understanding of the boundaries between the different distributions, shown in figures 14 and 15. In this paper we have merely pointed out the existence of these crossovers, without relating them to other characteristic energies such as the level spacing or Thouless energy. A detailed numerical investigation of the behaviour of these boundaries with system size and disorder remains to be carried out. Finally, it will be of interest to study the effect of fluctuations on the magnitude of the order parameter. For conventional superconductors, these can occur on a scale many orders of magnitude greater than the lattice constant and therefore need not induce significant level repulsion amongst states above the gap.

Acknowledgments

This work was supported in part by the EEC via an HCM grant, by the EPSRC, NATO, the Institute for Scientific Interchange and by a ΠΕΝΕΔ research grant of the Greek Secretariat of Science and Technology. The authors are also grateful to V C Hui, S J Robinson, J-L Pichard and B Kramer for some stimulating discussions about this work.

References

[1] Wigner E P 1955 *Ann. Math.* **62** 548; 1957 *Ann. Math.* **65** 203
[2] Dyson F, 1962 *J. Math. Phys.* **3** 140; 1962 *J. Math. Phys.* **3** 1199
[3] Porter C E 1965 *Statistical Theories of Spectra: Fluctuations* (New York: Academic)
[4] Brody T A, Flores J, French J B, Mello P A, Pandey A and Wong S S M 1983 *Rev. Mod. Phys.* **53** 385
[5] Mehta M L 1967 *Random Matrices and the Statistical Theory of Energy Levels* (New York: Academic)
[6] Berry M 1991 *Chaos and Quantum Physics (Les Houches Summer School Section LIV)* ed M-J Giannoni, A Voros and J Zinn-Justin (Amsterdam: North–Holland) p 251
[7] Bohigas O and Giannoni M J 1984 *Mathematical and Computational Methods in Nuclear Physics (Springer Lecture Notes in Physics)* ed J S Dehesa, J M Gomea and A Polls (Berlin: Springer) p 1
[8] Haake F 1991 *Quantum Coherence in Mesoscopic Systems* ed B Kramer (New York: Plenum) p 583
[9] Eckhardt B 1987 *Phys. Rep.* **163** 205
[10] Casati G (ed) 1985 *Chaotic Behaviour in Quantum Systems* (London: Plenum)
[11] Sivan U and Imry Y 1987 *Phys. Rev.* B **35** 6074
[12] Altshuler B L 1987 *Proc. 18th Int. Conf. on Low Temp. Physics; Japan. J. Appl. Phys. Suppl.* **26** 1938
[13] Al'tshuler B L, Zharekeshev I Kh, Kotochigova S A and Shklovskii B I 1988 *Sov. Phys.–JETP* **67** 625
[14] Shklovskii B I, Shapiro B, Sears B R, Labrianides P and Shore H B 1993 *Phys. Rev.* B **47** 11 487
[15] Evangelou S N 1994 *Phys. Rev.* B **49** 16 805
[16] Anderson P W 1958 *Phys. Rev.* **109** 1492
[17] Stone A D, Mello P A, Muttalib K A and Pichard J-L 1991 *Mesoscopic Phenomena in Solids* ed B L Al'tshuler, P A Lee and R A Webb (Amsterdam: North-Holland) p 369
[18] Melsen J A and Beenakker C W J 1994 *Physica* B **203** 219
[19] See, for example,
Bruun J T, Hui V C and Lambert C J 1994 *Phys. Rev.* B **49** 4010 and references therein
[20] Lambert C J 1991 *J. Phys.: Condens. Matter* **3** 6579
[21] Lambert C J, Hui V C and Robinson S J 1993 *J. Phys.: Condens. Matter* **5** 4187
[22] Andreev A F 1964 *Sov. Phys.–JETP* **19** 1228
[23] Hui V C and Lambert C J 1990 *J. Phys.: Condens. Matter* **2** 7303
[24] Hui V C and Lambert C J 1993 *J. Phys.: Condens. Matter* **5** 697